Concurrent detection of chemically modified bases in yeast mitochondrial tRNAs by Nanopore direct RNA sequencing

Julia L. Reinsch[1,2] and David M. Garcia[1,2,*]

1 Institute of Molecular Biology, University of Oregon, Eugene, OR, 97403, USA
2 Department of Biology, University of Oregon, Eugene, OR, 97403, USA

*Correspondence should be addressed to: dmgarcia@uoregon.edu

ABSTRACT

Mutations in tRNA-modifying enzymes are associated with severe mitochondrial disease in humans. *Saccharomyces cerevisiae* has been used to model the impact of these mutations due to enzyme conservation and the ease of phenotyping mitochondrial defects in yeast. Yet the mature sequences of all its mitochondrially-encoded tRNAs (mt-tRNAs), including the positions of chemically modified bases, have not been determined in their entirety. We used Nanopore direct RNA sequencing (DRS) of mitochondrially-enriched RNA combined with enzyme knockouts to map base modifications across 24 mt-tRNA isoacceptors in yeast. Analysis of mt-tRNAs from wild-type yeast revealed base miscalls that were coincident with known modification sites at annotated positions, as well as at previously undescribed sites. Comparison to yeast lacking the *PUS4* gene, which encodes a conserved pseudouridine synthase, demonstrated that 23 of 24 mt-tRNAs are pseudouridylated by Pus4 to form Ψ_{55} in the T-loop. We also mapped the uridines modified by Pus2, catalyzing Ψ_{27} and/or Ψ_{28} on several mt-tRNAs, a function matching its paralog Pus1 that modifies cytosolic tRNAs at the same positions. In yeast lacking the *PUS2* gene, some mt-tRNAs also showed changes at other positions inconsistent with being Pus2-pseudouridylated sites. These include U_{34} that is modified to $cmnm^5s^2U_{34}$ in the anticodon of mt-tRNA$^{Lys(UUU)}$, and A_{21} in mt-tRNA$^{His(GUG)}$ that is not previously known to be modified. Sequencing of a strain lacking the *DUS2* dihydrouridine synthase gene also permitted determination of the dihydrouridine sites catalyzed by Dus2. Loss of this D_{20} modification also led to pleiotropic effects on other putative modification sites, those presumed catalyzed by Dus1 and Trm1, in many mt-tRNAs. In summary these data provide a comprehensive analysis of *S. cerevisiae* mt-tRNA sequences, including modifications. They also suggest previously unknown RNA modification “circuits” in mt-tRNAs, in which loss of Pus2-catalyzed Ψ_{27}/Ψ_{28} and Dus2-catalyzed D_{20} causes increases or decreases in other modifications. Changes of multiple different modifications from loss of the activity of a single enzyme has implications for how mutations in these genes may cause pleiotropic effects on tRNA structure and translation.

INTRODUCTION

Eukaryotic organisms contain a nuclear genome in the form of linear chromosomes, and a mitochondrial genome, in the form of circular dsDNA molecules found in the mitochondrial matrix. Mitochondrial genomes are orders of magnitude smaller than nuclear genomes and are highly reduced derivatives of the bacterial genome from which they evolved (Bullerwell and Gray 2004). Most genes retained in mitochondrial genomes encode proteins involved in oxidative phosphorylation and are therefore essential for respiration. These are synthesized within mitochondria by a translation machinery that includes mitochondrially encoded rRNA and tRNA.

In most organisms examined, the mitochondrial-encoded tRNAs, “mt-tRNAs”, are necessary and sufficient to fully decode mitochondrial mRNAs (Huot et al. 2014). While there are some examples of cytosolic tRNAs being imported into *S. cerevisiae* mitochondria (Tarassov et al. 1995; Rinehart et al. 2005; Kamenski et al. 2007), the essentiality of this is controversial (Alfonzo and Söll 2009; Rubio and Hopper 2011). In general mitochondrial tRNAs adopt similar secondary/tertiary structures to those in bacteria and in the cytoplasm, with some exceptions (Krahn et al. 2020), but they usually contain fewer chemical modifications than found in cytosolic tRNA isoacceptors, although a similar number as found in bacterial isoacceptors (Machnicka et al. 2015).

A key difference between nuclear and mitochondrial tRNA genes is that nuclear genomes contain multiple genes encoding identical copies of most tRNA isoacceptors, while mt-tRNAs tend to be encoded by single-copy genes. In the genome of the budding yeast, *Saccharomyces cerevisiae*, there are 42 nuclear tRNA isoacceptors, with the number of gene copies ranging from 1–16 per tRNA (Percudani et al. 1997). In contrast, its mitochondrial genome encodes 24 tRNA isoacceptors, each encoded by a single gene copy.

During their biogenesis, mitochondrial tRNAs undergo post-transcriptional processing and modification steps that are conserved across life, including in bacterial tRNAs and eukaryotic cytosolic tRNAs: 1) They undergo cleavage of their 5´ and 3´ ends by RNase P and RNase Z, respectively, 2) They have a terminal 3´ CCA added through non-templated enzymatic synthesis (prokaryotic tRNAs have this feature genetically encoded), 3) They are chemically modified at various tRNA base positions by a myriad of enzymes. This study focuses on the tRNA base chemical modifications.

Chemical modifications to tRNA serve important roles in tRNA structure, stability and promotion of translation fidelity (reviewed in Suzuki 2021). Due to the fact that mt-tRNAs are necessary for decoding several genes essential for respiration, defects in the chemical modification of mt-tRNAs, catalyzed by a suite of enzymes, can lead to defects in cell growth and are responsible for several human diseases, often referred to as “modopathies” (Suzuki 2021; Magistrati et al. 2023). The state-of-the-art of comprehensive annotation of human mt-tRNA modifications was demonstrated in a study that individually purified all 22 human mt-tRNAs, and subjected each to mass spectrometric analysis (Suzuki et al. 2020). These types of approaches are incredibly important for establishing a map of what modifications are found on which isoacceptors and at what positions. Due to the elevated technical benchmark required for this approach, however, it is less amenable to investigate the impact of multiple cell or enzyme perturbations on these modifications.

The budding yeast *S. cerevisiae* has been a useful model system for investigating the enzymes that chemically modify mt-tRNA for a few reasons: 1) Yeast offers facile genetics, making it

straightforward to perturb functions of modification enzymes; 2) Yeast can survive by fermentation, making mitochondrial gene expression non-essential under appropriate growth conditions; 3) Many of the tRNA modifications and the enzymes that catalyze them are conserved with those in human mitochondria; 4) The relative ease of growing yeast cultures to obtain sufficient material for analysis. Various discoveries enabled by work in yeast has thus helped develop a mechanistic understanding of the basis of several human modopathies (Umeda et al. 2005; Wang et al. 2009; Baruffini et al. 2013; Powell et al. 2015). Nevertheless, characterization of yeast mt-tRNA modifications is incomplete, with the benchmark modification database, Modomics (Cappannini et al. 2024), providing modification profiles for only 16 of 24 yeast mt-tRNA isoacceptors. Thus, annotation of all mt-tRNA modifications in yeast will further our understanding of their role in mitochondrial function and disease.

With this in mind, we have pursued the relatively new approach of Oxford Nanopore Technologies (ONT) direct RNA sequencing (DRS) of full length tRNAs, permitting an *indirect* analysis of tRNA chemical modifications. This measurement can provide position-level resolution, but at increased throughput compared to mass spectrometric analysis. As RNA bases transition across a nanopore, chemically modified versions can lead to distinct ionic current signals compared to their unmodified counterparts. These ionic current changes often cause basecalling programs to artifactually assign a nucleotide to the modified position that does not match the “reference”, unmodified nucleotide. This signal is referred to as a base “miscall”, and certain modifications can produce distinct miscall patterns, such as pseudouridine typically causing a “U-to-C” miscall coincident with the modified position. While an indirect measurement, when coupled with appropriate biochemical and/or genetic controls, these miscall data are informative about the positions and identities of modified bases. This includes conditions that affect the cellular growth state or RNA modifying enzyme activities (Thomas et al. 2021; Lucas et al. 2023 Apr 6; Sun et al. 2023; White et al. 2023; Shaw et al. 2024; White et al. 2024). These data have also promoted an *in vivo* systems-level understanding of modification interdependencies across dozens of tRNAs (Shaw et al. 2024).

Mitochondrial tRNAs offer a particularly useful test case for the advancement of direct tRNA-sequencing because they contain many of the conserved tRNA modifications found across Eukarya, but at a lower density compared to cytosolic tRNAs, thus establishing more isolated base call signatures that advance further training and testing of DRS to interpret specific chemical modification identities. Using RNA from a mitochondria-enriched fraction of budding yeast, we analyzed yeast mt-tRNAs using DRS. We built our DRS-based sequence analysis on a revised complete structural alignment of budding yeast mt-tRNAs. By comparing our analysis to annotations on Modomics, we found that DRS is can detect signal for nearly all known yeast mt-tRNA modifications. Furthermore, we detected evidence of unknown modifications on several isoacceptors. Through genetic analysis we also discovered new examples of modification interdependencies, in which loss of one modification leads to increases or decreases in the levels of modifications at other positions.

RESULTS

Structural alignment of 24 *S. cerevisiae* mitochondrial tRNAs

A prerequisite to analyze the sequences and modifications of yeast mitochondrial tRNAs (mt-tRNAs) was generation of an updated reference list of mt-tRNA sequences, as well as a structural alignment to facilitate miscall-based modification analysis. During our study, Modomics contained

16 mt-tRNA sequences from *S. cerevisiae*, yet it was known that mitochondrial DNA encodes at least 24 mt-tRNA genes. For example, RNA-seq experiments to map the entire yeast mitochondrial transcriptome (Turk et al. 2013) calculated the 5´ and 3´ bounds of all mt-tRNAs. We compiled a revised reference set of sequences by performing pairwise comparisons of mitochondrial tRNA sequences annotated from that publication, Modomics (Cappannini et al. 2024), and NCBI (Wolters et al. 2015; Sayers et al. 2024). Most mt-tRNA sequences were identical among these sources, however we found that most mt-tRNAs from the NCBI database contained additional nucleotides at the 5´ and/or 3´ends. We removed these extra nucleotides from our reference based on our assumption that they were less likely to be present in natural sequences because they were not predicted to form additional base pairs at the "top" of the acceptor stem, and were not within the bounds determined by RNA-seq. In Supplemental Table S1 we provide our reference mt-tRNA sequences, which we note also include the common RNA bases of the 5´ splint adapter (Supplemental Table S2), followed by the mature mt-tRNA sequence, and then the common RNA bases of the 3´ splint adapter. We only analyzed tRNA sequences encoded in the mitochondrial genome and did not include tRNAs potentially imported into the mitochondria from the cytosol (Rinehart et al. 2005)._This was due to the fact that our enrichment protocol (see below) was not designed to stringently purify mitochondrial material from the cytosol and thus included a minority of sequenced reads mapping to many cytosolic tRNAs, thereby precluding identification of any imported molecules.

Next, we manually curated a structural sequence alignment of all 24 mt-tRNAs based on conserved tRNA structural features including loop length, stem length, and tertiary contacts (Fig. 1A). We adopted a conventional tRNA numbering scheme (Steinberg et al. 1993), with a few changes to accommodate predicted single nucleotide bulges and additional nucleotides in the D-loop and anticodon-loop. Overall, our predicted secondary structures were very similar to those in our previous analysis of the cytosolic tRNAs (Shaw et al. 2024), apart from these minor differences. As seen in the cytosolic tRNAs, the Serine and Leucine mt-isoacceptors are both of the "type II tRNAs", containing longer variable loops (Brennan and Sundaralingam 1976). In mitochondria, the Tyrosine tRNA also has a longer variable loop, unlike the cytosolic Tyrosine tRNA. We did not predict any mt-tRNAs with predicted secondary structures that were dramatically different from a canonical tRNA, such as missing the D-arm or unusually long variable regions, as has been observed in some animals and archaea (reviewed in Salinas-Giegé et al. 2015). Although we cannot rule out that such examples might exist in budding yeast, they would be less likely to be predicted by the tools that we used here. We used this structural alignment and numbering scheme, as displayed in Fig. 1A, in our analysis and display of our sequencing data below. We summarize the known modifications in yeast mt-tRNAs and their catalyzing enzymes, if known, in Fig. 1B.

Direct sequencing of 24 *S. cerevisiae* mitochondrial tRNAs

In our previous sequencing of total yeast tRNA isolated from wild-type cells grown in glucose and harvested during exponential phase (Shaw et al. 2024), the abundance of reads fully aligning to our mt-tRNA reference was 0.3% of total, while the remaining 99.7% mapped to a reference set of 42 cytosolic tRNA isoacceptor sequences. There were likely two primary reasons for the low output of mt-tRNA: 1) mitochondrial tRNAs are significantly less abundant than cytosolic tRNAs, and 2) yeast cells grown in media containing glucose as a principle carbon source contain fewer mitochondria than cells grown in carbon sources that require oxidative respiration, such as glycerol or ethanol (Miyakawa et al. 2004). To address these limitations, we grew yeast cells in 2% ethanol media, rather than 2% glucose media, to expand the pool of cellular mitochondria

further, and performed an enrichment for yeast mitochondria prior to RNA isolation (Fig. 2A**)**. We note that larger culture sizes (1L) were also necessary for obtaining enough enriched mitochondria material.

We isolated RNA molecules between 70 and 100 nt long from the mitochondrially-enriched RNA fraction using PAGE. Oligonucleotide splint adapters were ligated to this RNA pool, followed by ligation to the Oxford Nanopore Technologies (ONT) RNA sequencing adapter (Fig. 2B). The library of adapted tRNA molecules were sequenced with ONT MinION R9.4.1 flow cells and SQK-RNA002 kits. As a control for these cellular-derived tRNA molecules, we analyzed *in vitro* transcribed (IVT) tRNA sequences that contained no modifications and thus served as a reference for DRS signal obtained from otherwise identical tRNA sequences (See Materials and Methods for details about IVT sample, library preparation, and sequencing). The raw ionic current patterns were converted to nucleotide base calls using ONT Guppy software (version 3.0.3) (Fig. 2B**)**. Each of these tRNA DRS experiment yielded between 34,843 and 112,800 total reads per flow cell (Supplemental Table S3).

We aligned reads to a curated reference containing all 24 mitochondrial and 42 cytosolic yeast tRNA isoacceptors (Supplemental Table S1) using BWA-MEM (Li 2013). Each tRNA DRS experiment yielded between 15,337 and 63,709 MAPQ1-aligned tRNA reads per flow cell (Supplemental Table S3). The average percentage of mapped reads across experiments was ~51%, which is consistent with prior tRNA DRS experiments (Lucas et al. 2023; Shaw et al. 2024). Between 11,904 and 62,516 MAPQ1-aligned tRNA reads per flow cell exclusively aligned to mitochondrial tRNA reference sequences (Supplemental Table S3). This amounts to 77.9–98.1% mitochondrial tRNA reads, a substantial increase in sequencing depth (~300-fold compared to (Shaw et al. 2024) compared to prior tRNA DRS studies performed without mitochondrial enrichment (Shaw et al. 2024; White et al. 2024) and DRS of mitochondrial RNA without prior tRNA-specific capture (Koster et al. 2024) (Fig. 2C).

For these analyses, we used the now-discontinued R9.4.1 flow cells and RNA002 sequencing kits because 1) data collection began prior to the release of ONT “RNA” flow cells and RNA004 kits, and 2) to permit direct comparison to our recent DRS analysis of 42 yeast cytosolic tRNAs using the same chemistry and basecalling approach. Of note, the miscall-based modification detection using the RNA002 chemistry employed here was validated by orthogonal LC-MS/MS experiments in our prior study (Shaw et al. 2024). Miscall-based DRS analysis of tRNA chemical modifications has provided valuable biological insights in numerous studies already (Thomas et al. 2021; Lucas et al. 2023 Apr 6; Sun et al. 2023; White et al. 2023; Shaw et al. 2024; Riquelme-Barrios et al. 2025) and will continue to do so until direct ionic current analysis of DRS data is robust and widely adopted.

DRS reveals modification landscape of yeast mt-tRNAs

We used heatmaps containing reference match probabilities at each position in all 24 yeast mt-tRNAs to visualize base miscalls. The ‘reference match probability’ (RMP) at a given position in a tRNA represents the probability that the nucleotide assigned by the base caller matches the canonical unmodified reference nucleotide. These probabilities were calculated using an error-based model that accounts for standard DRS rates of mismatches, insertions, and deletions, as well as sequence context-based effects unique to the unmodified sequences that were derived from our IVT mt-tRNA data and other parameters (see Materials and Methods). The mt-tRNA IVT heatmap (Fig. 3A) shows that nearly all positions have a high RMP (dark blue) as expected from

unmodified RNA. The IVT sequences represent an important control dataset that accounts for DRS error that can arise from certain sequence contexts of unmodified RNA bases. For example, while position 42 in mt-tRNA$^{Asp(GUC)}$ here yielded a light colored square—frequently associated with a modification-triggered miscall—we verified that the DNA oligonucleotide used as the template to *in vitro* transcribe this tRNA matched the reference nucleotide, using Sanger sequencing (data not shown). Further inspection of the k-mer associated with this position, 5´-**G**GAGG-3´, in other IVT molecules revealed a common G-to-A miscall as we observed here (Shaw et al. 2024) thus implicating this sequence context as triggering the miscall and not some other anomaly. In contrast to the IVT data, in the heatmap showing wild-type mt-tRNAs isolated from yeast (Fig. 3B), while most positions remain dark blue, many positions spanning the D-loop to the T-loop are yellow-toned even after correction from the error model, indicating high frequency of base miscalls representing likely modification sites. There are notably fewer base miscalls in these mitochondrial tRNAs relative to cytosolic tRNAs analyzed with the same method (Shaw et al. 2024), in agreement with a recent literature review concluding fewer modifications, on average, for mt-tRNAs than cytosolic tRNAs in yeast (Phizicky and Hopper 2023).

Within the 16 previously annotated mt-tRNAs present in the Modomics database, 10 unique chemical modifications were documented in 16 different base positions (i.e. some modifications appear at more than one position, such as pseudouridine) (Supplemental Table S4) (Cappannini et al. 2024). We calculated the *mismatch* probability (equal to 1.0 minus the reference match probability value) for each position from a random subset of 105 aligned reads per mt-tRNA isoacceptor. In the program used to calculate posterior probabilities, marginCaller, the default posterior probability threshold to call an alternative nucleotide was empirically determined and set at 0.3 (Jain et al. 2015). Positions with a mismatch probability <0.3 in IVT and ≥ 0.3 in wild-type were classified as robust miscalls. Of the 16 documented modification sites, within our data 15 of them had a mismatch probability of ≥ 0.3 in at least one mt-tRNA annotated to have a modification at that position (Supplemental Table S5). The only annotated modification that was not detected on any mt-tRNA isoacceptor by DRS was m^5U_{54}, a result consistent with our prior sequencing of cytosolic yeast tRNAs, in which genetic deletion of this modification did not alter the DRS-based signal at positions known to contain it (Shaw et al. 2024). Therefore, as the vast majority of annotated modifications in mt-tRNAs (15 out of 16) produced a detectable *miscall-based* signal with our protocol, these data highlight the utility of DRS for profiling tRNA modifications. Given the strong correlation between mt-tRNA modifications as documented on Modomics with miscall-based signals in our DRS data, we extrapolated to the other eight mt-tRNAs whose ensemble of modifications were not previously documented. Our data supported these as containing approximately 5–8 predicted modifications each, a pattern resembling the other 16 isoacceptors, apart from the sparsely modified mt-tRNA$^{Asp(GUC)}$ that only produced miscalls at 2 positions (Supplemental Table S5). Most of these eight mt-tRNAs likely also contain Trm2-catalyzed m^5U_{54}, as 15 of 16 mt-tRNA isoacceptors listed on Modomics contain this modification (Cappannini et al. 2024). In addition to detecting annotated modification sites in the previously documented isoacceptors, our data also revealed putative novel modifications at several sites, some discussed below. Among known mt-tRNA modifications, pseudouridines were the most robustly detected by miscalls in our DRS data, and therefore much of our subsequent analysis below focuses on this modification, and its impact on others.

Pseudouridine can be detected as a U-to-C miscall at the modified position that does not impact miscalls at neighboring, unmodified positions (Begik et al. 2021). Annotated Ψ sites at positions 27, 28, 31, and 55 are reflected by miscalls in 100% of the positions previously annotated to

contain them, while Ψ sites at positions 32 and 39 were represented by miscalls in 83% of isoacceptors previously annotated to contain them (Supplemental Table S4). The only previously annotated Ψ position that our data did not recapitulate was position 72 of mt-tRNA$^{iMet(CAU)}$, which could be due to differences in growth conditions as our cells were grown in ethanol as a carbon source while the original study used galactose (Schneller et al. 1976; Canaday et al. 1980). Indeed, our prior work found that yeast growth conditions can influence the levels of other modifications as detected by DRS (Shaw et al. 2024). Finally, these data identified 21 sites likely to be pseudouridylated in the eight unannotated mt-tRNAs, based on comparison to pseudouridylated positions known in the 16 annotated mt-tRNAs. We subsequently validated 11 of these 21 sites through genetic knockouts of pseudouridine synthase (Pus) enzymes (see below).

Pus4 pseudouridylates 23 of 24 *S. cerevisiae* mt-tRNAs at U_{55}

In the yeast cytosol, the Pus4 enzyme catalyzes formation of U_{55} to Ψ_{55} for 41 of 42 tRNA isoacceptors (Shaw et al. 2024). Pus4 also modifies mt-tRNAs (Becker et al. 1997) and all 16 of the yeast mt-tRNAs with known sequences and modification profiles contain Ψ_{55} (Cappannini et al. 2024). We sequenced mitochondria-enriched tRNAs from yeast lacking the *PUS4* gene to verify that the low reference match probability at U_{55} shown in the heatmap of wild-type mt-tRNAs (Fig. 3B) was due to Pus4-catalyzed Ψ. In mt-tRNAs isolated from this *pus4*Δ strain, there was a high reference match probability at position 55 (Fig. 4A), which indicates a lack of modification. The subtractive heatmap shown in Fig. 4B highlights differences in reference match probability between mt-tRNA isolated from wild-type and *pus4*Δ yeast strains, where blue colored squares represent a decrease in modification in the mutant. Out of the 24 yeast mt-tRNAs, we found that 23 were modified at position 55 by Pus4 (Supplemental Table S6). The exception was mt-tRNA$^{Asp(GUC)}$ which has a guanosine at position 55 and therefore cannot be pseudouridylated at this site.

Some tRNA modifications are involved in "circuits" where one modification promotes the formation of other modifications (Porat 2025). A well-studied modification circuit involves Pus4-catalyzed Ψ_{55} that promotes the addition of m^1A_{58} in the T-loop of many yeast cytosolic tRNAs (Barraud et al. 2019; Yared et al. 2023; Shaw et al. 2024). The enzyme complex that catalyzes the formation of m^1A_{58} in cytosolic tRNAs—Trm6 and Trm61—is not known to localize to budding yeast mitochondria (Morgenstern et al. 2017; Di Bartolomeo et al. 2020), and no budding yeast mt-tRNAs are annotated to contain this modification (Cappannini et al. 2024). Our data support the view that the m^1A_{58} does not occur in these mt-tRNAs, as we did not detect miscalls associated with m^1A_{58} in any of the 24 mt-tRNAs. Furthermore, we did not find evidence of any other modification circuit initiated by Pus4, as there were no additional changes beyond the 55th position in cells deleted for the *PUS4* gene (Fig. 4B).

Identification of Pus2 pseudouridylation sites in *S. cerevisiae* mt-tRNAs

The mitochondrially-localized enzyme Pus2 is known to modify U_{27} and U_{28} of mt-tRNAs while its paralog Pus1 modifies cytosolic tRNAs at the same positions in budding yeast (Motorin et al. 1998; Behm-Ansmant et al. 2007). Seven of the 16 yeast mt-tRNAs currently on Modomics are annotated to contain Ψ at position 27 or 28 (Cappannini et al. 2024), but only sites on mt-tRNA$^{Arg(UCU)}$ and mt-tRNA$^{Lys(UUU)}$ have been determined to be Pus2-dependent (Behm-Ansmant et al. 2007). We sought to map Pus2 sites on all 24 mt-tRNAs by sequencing mitochondria-enriched

tRNA isolated from yeast with a deletion of the *PUS2* gene (Supplemental Fig. S1A). We assigned Pus2 sites by qualitatively examining the *pus2*Δ - wild-type subtractive heatmap (Fig. 5A), followed by a comparison of mismatch probabilities between the strains (Supplemental Table S5). For position U_{27} or U_{28}, if the mismatch probability was equal to or greater than the 0.3 threshold in the wild-type data, less than 0.3 in the *pus2*Δ data, and the change in mismatch probability met an empirically determined minimum difference threshold (see Materials and Methods), we reasoned that the change was caused by a Pus2-dependent Ψ. This analysis corroborated all seven previously annotated Ψ_{27}/Ψ_{28} sites, and we determined that Pus2 modifies six of these sites (Supplemental Table S6). The exception was U_{27} of mt-tRNA$^{Thr(UAG)}$, where the mismatch probability was above 0.3 at position 27 in both wild-type and *pus2*Δ. This miscall is likely caused by Ψ as previously annotated (Sibler et al. 1981), but our approach did not support that Pus2 is the specific pseudouridine synthase that modifies mt-tRNA$^{Thr(UAG)}$ at this site. Analysis of this isoacceptor from cells deleted for additional Pus enzymes may clarify this annotation. We also cannot exclude the possibility that this site *is* modified by Pus2, but in its absence, another synthase ectopically modifies it, leading to the higher mismatch probability in *pus2*Δ cells. Additionally, we inferred the presence of a Pus2-dependent Ψ_{27} for three mt-tRNAs which have not been annotated until now: mt-tRNA$^{Asn(GUU)}$, mt-tRNA$^{Thr(UGU)}$, and mt-tRNA$^{Val(UAC)}$ (Supplemental Table S6). For mt-tRNA$^{Thr(UGU)}$, there is also a Pus2-dependent miscall at U_{28}, which would make it the only mt-tRNA to have Ψ at both position 27 and 28, a feature that is known to exist in Pus1-catalyzed sites in cytosolic tRNAs, e.g. in tRNA$^{Lys(UUU)}$, tRNA$^{Val(CAC)}$ and tRNA$^{Trp(CCA)}$ (Cappannini et al. 2024; Shaw et al. 2024). Another possibility is that this signal is due to bleed through from Ψ_{27}, but this will need to be resolved by an orthogonal method.

Pus2-catalyzed Ψ_{27} and Ψ_{28} impact other modification sites

In addition to detecting annotated modification sites in previously documented isoacceptors, our data also revealed putative novel modifications at several sites. Some of these base miscalls became more evident when they changed in response to an enzyme deletion. For example, our sequencing of mt-tRNA from yeast lacking Pus2 revealed that loss of Ψ_{27}/Ψ_{28} also induced changes in base miscalls at other sites, not previously known to be chemically modified by Pus2. These changes therefore implicated Pus2 in such modification "circuits", or instances in which addition of one modification promotes or represses addition of a second, different modification (Han and Phizicky 2018; Porat 2025). In mt-tRNA$^{His(GUG)}$, there was a large increase in reference match probability at A_{21} in *pus2*Δ relative to wild-type, which suggests that the addition of Ψ_{27} by Pus2 promotes the formation of an unknown/novel modification at/near A_{21}. The change in miscall at A_{21} was not dependent on the dihydrouridine signal from the adjacent position 20 (see below), therefore we do not believe that this was due to a change in dihydrouridine modification. This putative modification circuit therefore represented an example in which one modification promotes the addition of another modification.

However, our data also revealed several examples involving Pus2 in which the loss of Ψ_{27}/Ψ_{28} lead to an associated *increase* in a putative modification at a different site. In this type of circuit, one modification inhibits the formation of another one. This is demonstrated by mt-tRNA$^{Lys(UUU)}$, where the reference match probability at positions 34 and 35 were lower in *pus2*Δ compared to wild-type, suggesting that loss of Ψ_{28} leads to associated increase in a putative modification at a different site. We hypothesized that this change was caused by an increase in levels of the annotated modification cmnm^{5}s^{2}U at position 34 of the mt-tRNA$^{Lys(UUU)}$ anticodon. To test this, we used APM-PAGE followed by Northern Blotting to measure 2-thiolation levels of mt-tRNA$^{Lys(UUU)}$

in wild-type and *pus2*Δ strains (Supplemental Fig. S2). The results, however, indicated that the loss of Ψ_{28} does not alter 2-thiolation levels of mt-tRNA$^{Lys(UUU)}$, which refuted our initial hypothesis. It is possible that the increase in miscalls was due to increased levels of the non-thiolated portion of this modified uridine, the cmnm^{5}U, which is present in the anticodon of tRNA$^{Lys(UUU)}$ at a relatively low stoichiometry in wild-type cells, as compared to other modifications, (Umeda et al. 2005). This particular modification is not detected by APM-PAGE. Alternatively, the change in miscall could have been caused by the addition of a different modification not previously annotated at position 34/35 in this isoacceptor. It is unclear what impact a change in modification at this position would have on the ability of mt-tRNA$^{Lys(UUU)}$ to decode mRNA codons, although studies have found that cmnm^{5}U$_{34}$, s^{2}U$_{34}$, and cmnm^{5}s^{2}U$_{34}$ promote mt-tRNA$^{Lys(UUU)}$ charging and mitochondrial protein synthesis (Umeda et al. 2005; Wang et al. 2010). Finally, we found that Pus2 was involved in putative circuits in mt-tRNA$^{Thr(UAG)}$ and mt-tRNA$^{Thr(UGU)}$, where the reference match probability was decreased at position 31 or 30, respectively, when cells were missing Pus2 and thus the Ψ_{27}/Ψ_{28} modification. Position 31 is annotated as Ψ in mt-tRNA$^{Thr(UAG)}$ (Cappannini et al. 2024), while position 30 of mt-tRNA$^{Thr(UGU)}$ is a guanosine, which is a position not known to be modified in any yeast tRNA.

Identification of Dus2 dihydrouridylation sites in *S. cerevisiae* mt-tRNAs

All 16 mt-tRNA isoacceptors currently on Modomics are annotated to contain dihydrouridine (D) at position 20, yet its catalyzing enzyme on these tRNAs has not been confirmed experimentally. It has long been presumed that Dus2, which is responsible for dihydrouridylating position 20 in yeast cytosolic tRNAs (Xing et al. 2004), also modifies mitochondrial tRNAs at the same position. This hypothesis is supported by the detection of Dus2 in the yeast mitochondrial proteome (Morgenstern et al. 2017; Di Bartolomeo et al. 2020). Our DRS analyses of mt-tRNAs from *dus2*Δ yeast provide experimental evidence that Dus2 is, in fact, necessary for D$_{20}$ formation in mt-tRNAs. In cells deleted of Dus2, we observed a decrease in modification (increase in reference match probability) at position 20 and/or neighboring positions 19 and 20a/20b/21 for many mt-tRNAs (Supplemental Fig. S1B; Fig. 5B, blue squares). Therefore, a three-position window, centered on position 20, was considered for our analysis of mismatch probabilities, such that a threshold change at any one or more of these positions lead us to assign a D$_{20}$ (see Materials and Methods for details). We note that this three-position window has been observed for other genetically validated modifications, such as m^{1}A$_{58}$ (Shaw et al. 2024). Of the 16 mt-tRNAs in Modomics annotated to contain D$_{20}$, DRS corroborated 13 sites as Dus2 targets (Supplemental Table S6), indicating that DRS is a robust method for detecting dihydrouridine in this context. The three mt-tRNAs annotated to contain D$_{20}$ sites that were not detected by DRS were: mt-tRNA$^{Pro(UGG)}$, mt-tRNA$^{His(GUG)}$, and mt-tRNA$^{Tyr(GUA)}$. The mismatch probabilities in the position 20 window was below 0.3 for mt-tRNA$^{Pro(UGG)}$ in both wild-type and *dus2*Δ datasets. It is possible that mt-tRNA$^{Pro(UGG)}$ is modified by Dus2 under different growth conditions, or the stoichiometry of the modification is too low to be detected by DRS. Position 21 of mt-tRNA$^{His(GUG)}$ has a high mismatch probability (>0.8) in both wild-type and *dus2*Δ, which suggests that Dus2 is not responsible for this miscall. The identity of the modification causing the miscall at this A$_{21}$ of mt-tRNA$^{His(GUG)}$ is unknown, and there are no modifications documented at position 21 for any yeast tRNA (Cappannini et al. 2024). For mt-tRNA$^{Tyr(GUA)}$, the mismatch probability at position 20a was greater than 0.3 in the IVT, wild-type, and *dus2*Δ experiments. The mismatch probability at 20a in the wild-type data was higher (0.708) than in the *dus2*Δ (0.468) data, which suggests a modification is likely present here in mt-tRNA$^{Tyr(GUA)}$. However, since the mismatch probability at position 20a was above 0.3 in the *dus2*Δ data, we did not categorize mt-tRNA$^{Tyr(GUA)}$ as a Dus2 substrate, but

recognize that an alternative method such as “D-seq” (Draycott et al. 2022) may clarify this annotation.

Our analysis of the eight mt-tRNAs not currently on Modomics revealed that six additional mt-tRNAs contain a Dus2-dependent D_{20} (Supplemental Table S6). Neither mt-tRNA$^{Asp(GUC)}$ nor mt-tRNA$^{Cys(GCA)}$ had a miscall at position 20 or its neighboring positions, despite the presence of a uridine-20 that could act as a substrate for Dus2. These mt-tRNAs contain unique structural/sequence features in the D-loop including the lack of G_{18} in mt-tRNA$^{Asp(GUC)}$ and the presence of a uridine at position 13a in tRNA$^{Cys(GCA)}$ (Fig. 1A). It is possible that these unusual differences repress Dus2 activity on these mt-tRNAs.

mt-tRNAs lacking D_{20} have increased modification levels at Dus1 and Trm1 sites

Dus2 initiated the most prevalent and striking examples in which the loss of modification at one site was accompanied by an increase in modification at nearby sites. For nearly every mt-tRNA with a decrease in miscalls at position 20 in *dus2*Δ, there is an increase (orange-colored boxes) in miscall levels at positions 15/16 or position 26 (Fig. 5B). The increase in miscalls at positions 15 and 16 are likely due to activity of Dus1. Dus1 modifies yeast cytosolic tRNAs at positions 16 and 17 (Xing et al. 2004) and has been detected in the yeast mitochondrial proteome (Morgenstern et al. 2017). Dihydrouridine is known to confer flexibility to the D-loop (Dalluge et al. 1996) and to increase the overall stability of tRNA tertiary structure (Dyubankova et al. 2015). Therefore, in the absence of Dus2, an increase in dihydrouridylation at positions 16/17 may be required to stabilize mt-tRNA tertiary structure. mt-tRNA$^{Lys(UUU)}$ and mt-tRNA$^{Phe(GAA)}$ had increased mismatch probabilities at position 26 when they lacked D_{20}. In the case of mt-tRNA$^{Phe(GAA)}$, this may be caused by an increase of the annotated $m^{2,2}G$ modification, catalyzed by Trm1 (Ellis et al. 1986). However, mt-tRNA$^{Lys(UUU)}$ contains an adenosine at position 26; since Trm1 is not known to or predicted to methylate adenosine bases, the identity of the putative modification at this site is unclear. We have also observed increases in miscalls at positions other than D_{20} sites in our DRS data from *dus2*Δ cytosolic tRNAs (unpublished data). Despite dihydrouridine’s important contribution to tRNA tertiary structure, all four Dus enzymes in yeast can be simultaneously deleted without substantial phenotypic consequences (Xing et al. 2004). It is possible that in the absence of dihydrouridine sites, levels of other modifications increase to compensate for changes in tRNA structure. Further research is needed to characterize interactions between dihydrouridine and other modifications in mt-tRNAs and their contributions to tRNA structure and mitochondrial function.

DISCUSSION

As DRS is increasingly applied to study tRNAs from a variety of species and cell-types, it remains important to define reference sequences for each case, even while allowing for the *de novo* discovery of new sequences that may be captured and have not been predicted or experimentally verified previously. Examination of mitochondrial tRNA sequences, as done here, may represent one of the simplest cases, for several reasons: 1) A smaller number of tRNA sequences (e.g. 24 yeast mt-tRNAs vs. 42 yeast cytosolic tRNAs), 2) Only a single gene copy for each tRNA in the mitochondrial genome, eliminating the complexity of accounting for isodecoders common in nuclear-encoded tRNA gene copies, 3) fewer chemical modifications compared to nuclear-encoded tRNAs. After we updated and expanded the current list of aligned mt-tRNA sequences from *S. cerevisiae*, we used this reference to profile miscall-associated chemical modifications, including identifying which specific positions are modified by three enzymes, Pus4, Pus2 and

Dus2. This genetics-informed approach then permitted us to predict evidence of instances in which the presence of one modification either stimulates or represses modifications at adjacent sites.

Our DRS approach could be used to model the effects of human disease-associated mutations in tRNA modification enzymes known to impact mitochondrial function. Most tRNA enzyme functions and even catalytic site sequences are conserved from yeast to humans. Testing mutations at orthologous sites in yeast proteins, or replacing the yeast proteins with their human counterparts and examining the impacts of mutations on tRNA modification activities in yeast mt-tRNAs is likely to expand our understanding of how these mutations affect mitochondria tRNA function and translation. Our findings also highlight how reduction or loss of a modification can lead to collateral effects on other modifications, sometimes decreases, sometimes increases, and the ensemble of these changes must be considered in context of the resulting molecular and physiological phenotype.

For example, mutations in the human PUS1 gene—whose encoded protein is alone responsible for modifying both cytoplasmic and mitochondrial tRNAs—have been linked to the disease Myopathy Lactic Acidosis Sideroblastic Anemia (MLASA). It is not known whether the MLASA phenotype is due to reduced modification of cytoplasmic tRNAs, mitochondrial tRNAs, or the combination of both (Patton et al. 2005; Fernandez-Vizarra et al. 2007; Metodiev et al. 2015; Mangum et al. 2016) Our data showed that loss of Pus2-catalyzed pseudouridylation lead to changes to other modifications, consistent with a circuit. Analysis of human cells lacking PUS1 activity will be required to determine whether this also leads to changes in other modifications besides pseudouridine—as predicted from our work—in human mt-tRNAs, that may contribute to the disease phenotype. DRS presents an approach that could be used to address this unknown.

Our analysis of mt-tRNAs from cells lacking the *PUS2* gene showed that mt-tRNA$^{Thr(UAG)}$ and mt-tRNA$^{Thr(UGU)}$ had putative increases in modification levels at positions 31 and 30, respectively. We propose that the loss of Ψ_{27}/Ψ_{28} may decrease the stability of the anticodon stem in these tRNAs, leading to compensatory changes to modifications at positions 31/30. mt-tRNA$^{Thr(UAG)}$ has an enlarged 8-nt anticodon loop (Su et al. 2011), and we predict that the anticodon stem of mt-tRNA$^{Thr(UGU)}$ ends with U_{31} and U_{39} (Fig. 1A), which would not form a base pair if unmodified. Therefore, these tRNAs may be particularly sensitive to the loss of modifications in the anticodon stem due to these unique structural features.

Our study is the first to use DRS to profile dihydrouridine in tRNA using a genetic mutant of a Dus enzyme. Dihydrouridine is the second most abundant tRNA modification, after pseudouridine, and it's catalyzed by a family of Dus enzymes conserved across kingdoms of life. Dihydrouridine is known to stabilize overall tRNA tertiary structure (Dyubankova et al. 2015; Nomura et al. 2016), and the widespread changes to positions overlapping with Dus1 activity we saw upon deleting Dus2 suggests that these mt-tRNAs may be undergoing compensatory changes in modification that may be necessary to optimize overall tRNA structure and function. Our work also sets a benchmark for analyzing dihydrouridine more generally using DRS. Bacterial Dus activity has been shown to be sensitive to redox conditions (Kilz et al. 2024), and thus DRS could also be used to measure whether dihydrouridine could be regulated by oxidative stress in mt-tRNAs in yeast and other eukaryotes.

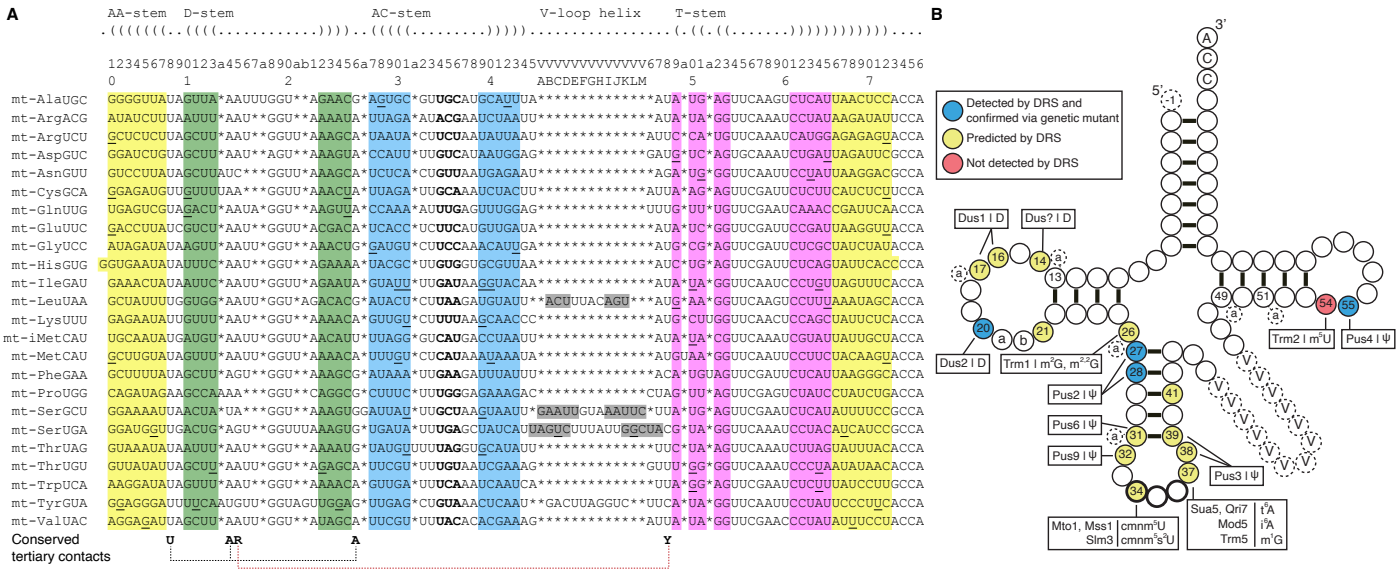

FIGURE 1. Budding yeast mitochondrial tRNA (mt-tRNA) sequences and the ensemble of their modifications profiled in this study. (*A*) Structured sequence alignment of 24 mt-tRNA isoacceptors from *S. cerevisiae*. Each base position of the alignment matches a box in the heatmaps presented in Figures 3–5. Asterisks indicate gaps. Left and right parentheses and colored regions show predicted helices/stems (labeled at top). Numbers (top line) indicate each base position in a repeating series of ~ten, or in bottom line every ~tenth position. Variable loop is up to 13 base positions in length, and alignment of these bases, as well as neighboring positions 44–48, in the Leucine, Serine and Tyrosine isoacceptors, were anchored via predicted helices/stems in the loop. Histidine tRNA contains a "-1" G added post-transcriptionally (Cappannini et al. 2024). G•U wobbles are included in predicted stem regions and underlined. Conserved tertiary contacts are indicated underneath the alignment (R=purine, Y=pyrimidine). (*B*) Secondary structure-based illustration of a generic yeast mt-tRNA, highlighting overall structural segments, ten types of known chemical modifications, and the names of single enzymes or heteromeric complexes annotated to catalyze them. Positions in blue are those that contain modifications verified in this study by their corresponding genetic mutants. Positions in yellow are those that also trigger base miscalls and are predicted to be chemically modified bases in at least one isoacceptor in this study . Position 54 (red) is annotated to be modified to m^5U for many mt-tRNAs, but this modification does not yield a base miscall coincident with this position, as previously documented (Shaw et al. 2024).

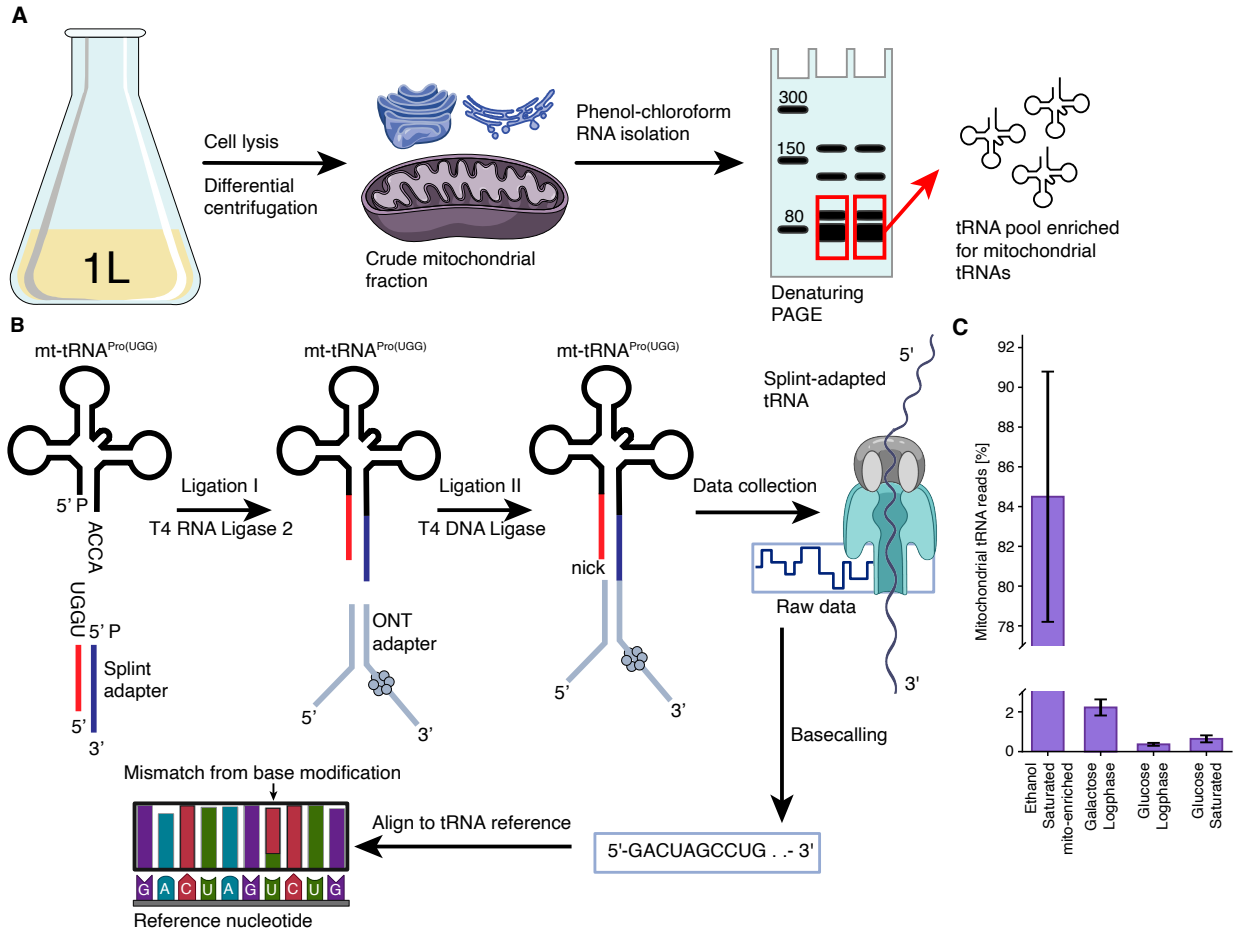

FIGURE 2. Overview of sample preparation and tRNA library preparation and sequencing. (*A*) Crude mitochondrial fraction from large yeast cultures is subjected to traditional RNA isolation, followed by gel purification of tRNA fraction. (*B*) tRNAs are ligated to a double-stranded splint adapter with T4 RNA Ligase 2 by the tRNA's 3´ NCCA overhang. A second ligation is performed using T4 DNA Ligase with the tRNA and ONT sequencing adapters. The splint-adapted tRNA pool is sequenced and based called as described in Materials and Methods. Base miscalls are analyzed to infer presence of chemical base modifications, using an IVT mt-tRNA library as a background model. (*C*) The full length mt-tRNA fraction from wild-type cells, as measured by DRS, was enriched ~300-fold versus a protocol lacking prior enrichment of mitochondria and different growth conditions (Shaw et al. 2024).

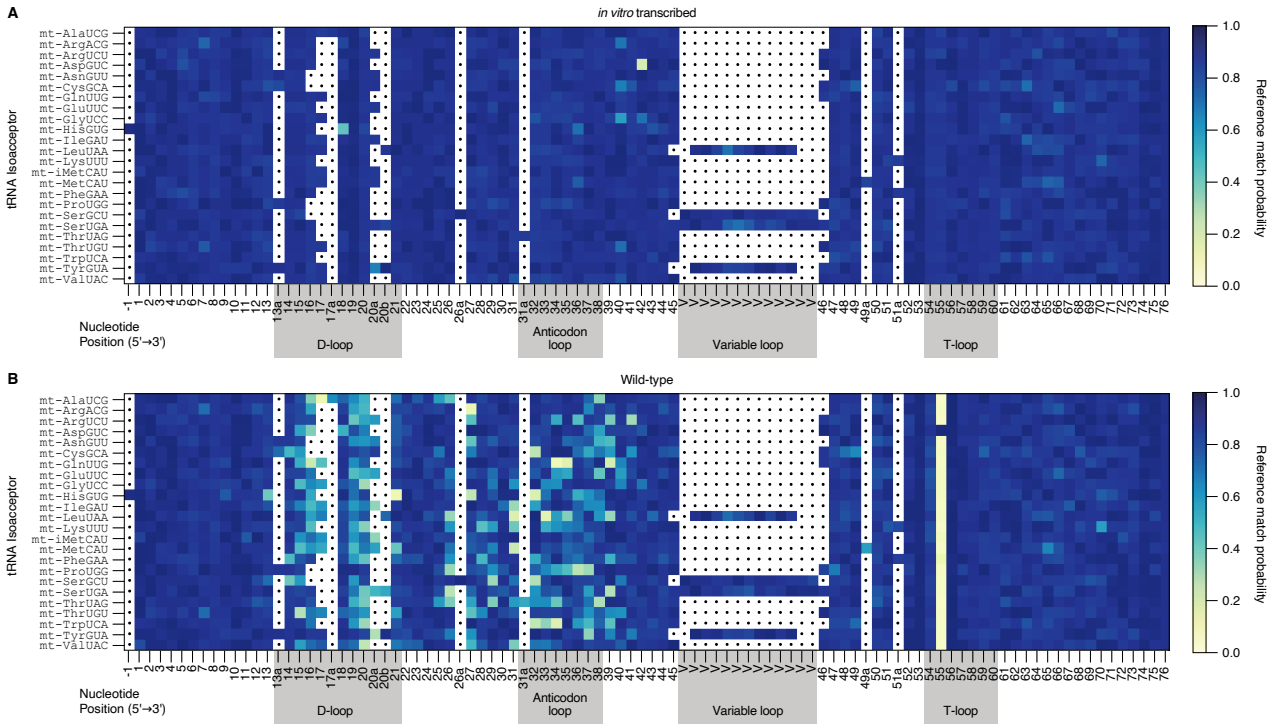

FIGURE 3. Heatmaps representing alignments of 24 *S. cerevisiae* mt-tRNA isoacceptors exhibit miscalls coincident with chemically modified positions. (*A*) Heatmap representing *in vitro* transcribed (IVT) tRNA sequences of 24 *S. cerevisiae* mitochondrial isoacceptors. A higher reference match probability (dark blue) corresponds to positions where the base-called nucleotide more frequently concurs with the reference nucleotide given the alignment, and a lower reference match probability (light yellow) corresponds to positions where the base-called nucleotide more frequently disagrees with the reference nucleotide. Sequences were aligned by the D-loop, anticodon loop, variable loop, and T-loop (grey boxes). Positions are numbered according to a conventional tRNA base numbering scheme, based on the sequence alignment in Figure 1A. (*B*) Wild-type isoacceptors isolated from yeast cells. Otherwise as described above.

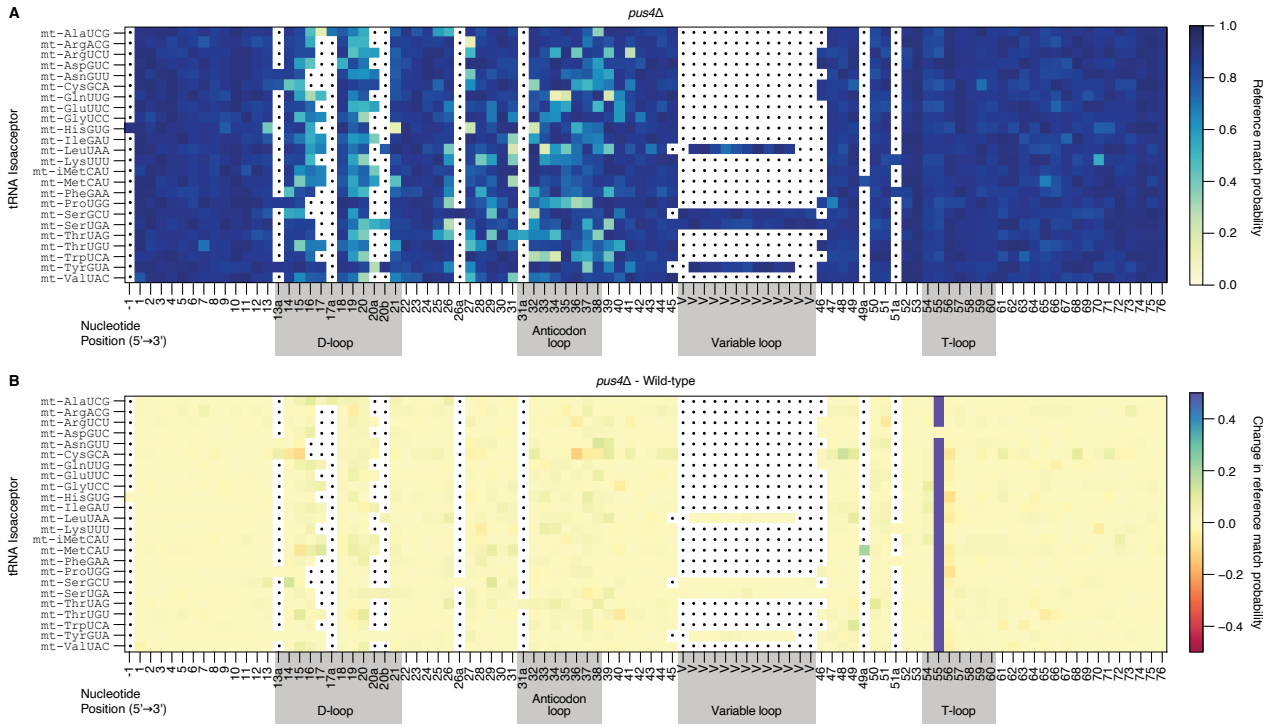

FIGURE 4. Heatmaps demonstrate Pus4-based pseudouridylation of 23 of 24 yeast mt-tRNA isoacceptors. (*A*) Heatmap representing mt-tRNAs from *pus4*Δ cells. Otherwise as described in Figure 3. (*B*) The change in reference match probabilities between *pus4*Δ and wild-type aligned isoacceptors. A positive change in reference match probability (blue/purple squares) indicates a decrease in base miscalls for *pus4*Δ, and a negative change in reference match probability (orange/red squares) indicates an increase in base miscalls for *pus4*Δ. Yellow squares indicate that basecalls do not differ between the two strains.

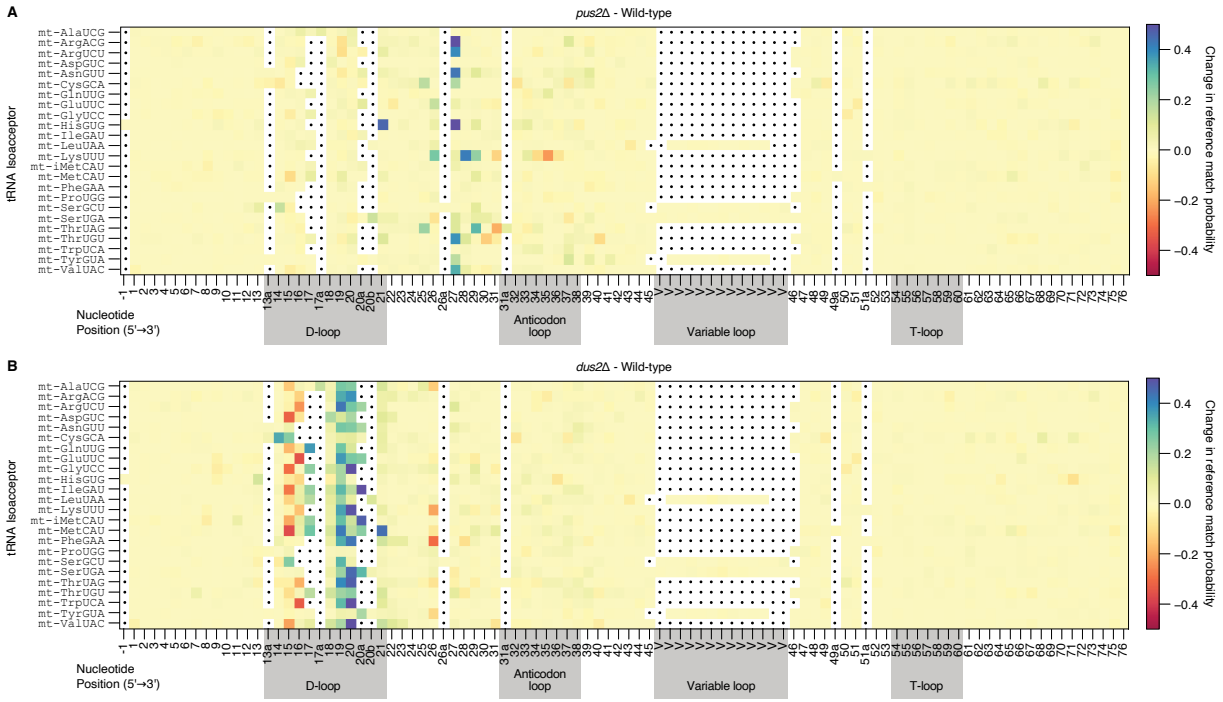

FIGURE 5. Heatmaps reveal modifications catalyzed by Pus2 and Dus2 impact other sites. The heatmaps show the change in reference match probabilities between (*A*) mt-tRNAs from *pus2*Δ and wild-type cells, and (*B*) mt-tRNAs from *dus2*Δ and wild-type cells. Otherwise as described in Figure 4B.

MATERIALS AND METHODS

Yeast growth conditions

See Supplemental Table S7 for yeast strains used in this study and their genotypes. Yeast strains were streaked out from the -80°C freezer onto YPD plates and grown for 2 days at 30°C. Individual colonies were picked to inoculate Xml culture tubes containing 5 mL of YPD media. The liquid cultures were grown overnight on a roller drum wheel at 30°C. The next morning the cultures were diluted 1000-fold into 50 mL of YPD media in 250 mL Erlenmeyer flasks. The cultures were grown overnight on a shaking incubator at 300 rpm and 30°C. The yeast were centrifuged in 50 mL conical tubes at 3000g for 5 min at room temperature. The supernatant was removed, and the pellets were resuspended in 20 mL YPE (Yeast extract, Peptone, 2% Ethanol) media and added to 980 mL YPE in 3 L Erlenmeyer flasks with a baffled base for increased aeration. The cultures were grown on a shaking incubator at 300 rpm and 30°C for ~36 hours, until an OD_{600} of 1.0-1.4 was reached. The yeast were centrifuged in 1000 ml Nalgene centrifuge bottles at 3000g for 5 min at room temperature. The supernatant was poured off and the yeast pellets were resuspended in 250 mL of sterile Millipore water and centrifuged again at 3000g for 5 min at room temperature. The supernatant was removed, and the cells were resuspended in 45 mL of 1X PBS, then transferred to 50 mL conical tubes. The resuspended cells were centrifuged at 3000g and 4°C for 5 min and the supernatant was decanted. The pellets/conical tubes were immediately submerged into liquid nitrogen to flash freeze, then stored at -80°C.

Crude mitochondrial fraction isolation

The crude mitochondrial fraction was isolated from yeast cells using differential centrifugation as previously described (Meisinger et al. 2005; Gregg et al. 2009). The yeast pellets were thawed on ice, resuspended in 45 mL water and centrifuged at 3000g at room temperature for 5 min. The supernatant was decanted, and the wet weight of each cell pellet was recorded. The cell pellets were resuspended in 2 mL of DTT buffer (100 mM Tris-H_2SO_4 (pH 9.4), 10 mM dithiothreitol) per gram (wet weight) of cells. The tubes were placed on a shaker at 70 rpm and 30°C for 20 min. The cells were centrifuged at 3000g, room temperature for 5 min. The cell pellets were resuspended in 7 mL Zymolyase buffer (20 mM potassium phosphate (pH 7.4), 1.2 M sorbitol), without Zymolyase, per gram of cells. The cells were centrifuged (3000g, 5 min, 20°C), and the supernatant was decanted. The cells were resuspended in the same volume (7mL/g cells) of Zymolyase buffer and transferred to a 250 mL Erlenmeyer flask. 1 mg of Zymolyase 100T powder (United States Biological Corporation) per gram of cells was added to the cell suspension. The flasks were placed on a shaker at 70 rpm for 30 min at 30°C. The resulting mixture, which contained spheroplasts from cell wall digestion by Zymolyase, was transferred to 50 mL conical tubes and centrifuged (2200g, 8 min, 4°C). The supernatant was decanted. The pellet was carefully resuspended in 6.5 mL ice-cold homogenization buffer (10 mM Tris-HCl (pH 7.4), 0.6 M sorbitol, 1 mM EDTA, 0.2% (w/v) BSA) per gram of cells. The spheroplasts mixture was centrifuged (2200g, 8 min, 4°C) and the supernatant was decanted. The same volume of homogenization buffer (6.5 mL/g of cells) was used to resuspend the spheroplasts mixture, which was then transferred to a pre-chilled, dounce glass homogenizer on ice. With a tight ("B") pestle, the spheroplasts mixture was homogenized with 15 strokes. An equal volume of ice-cold homogenization buffer was added to the homogenizer, and then the homogenate was transferred to 50 mL conical tubes on ice. The homogenate was centrifuged (1500g, 5 min, 4°C) to pellet undigested cells, nuclei, and other large debris. The supernatant was poured into a new 50 mL conical tube and centrifuged (3000g, 5 min, 4°C) to further clarify the desired material. The

resulting supernatant was poured into a new 50 mL conical tube and centrifuged (12,000g, 15 min, 4°C) to pellet the mitochondria. The supernatant was decanted, and the pellet was resuspended in 6.5 mL ice-cold homogenization buffer per gram of cells, using trimmed pipette tips to avoid breaking organelles during resuspension. The two previous centrifugation steps (3000g, 5 min, 4°C and 12,000g, 15 min, 4°C) were repeated once to remove any remaining large debris, and to re-pellet the mitochondria. The supernatant was decanted and the crude mitochondrial fraction (also containing organelles including the endoplasmic reticulum, Golgi, and vacuoles (Meisinger et al. 2005)) was resuspended in 3 mL ice-cold SEM buffer (10 mM MOPS-KOH (pH 7.2), 250 mM sucrose, 1 mM EDTA). The crude mitochondrial fraction samples were stored overnight at 4°C in SEM.

tRNA isolation

The crude mitochondrial fractions were transferred to microcentrifuge tubes and centrifuged (12,000g, 15 min, 4°C) to pellet the mitochondria. The supernatant was removed, and the mitochondria were resuspended with 400 µL TES buffer (10 mM Tris (pH 7.5), 10 mM EDTA, 0.5% SDS). 400 uL of acidic phenol was added, and the tubes were incubated in a water bath at 65°C for 60 min, with 10 sec of vortexing every 15 min to lyse the mitochondria. The lysates were placed on ice for 5 min, then centrifuged (13,000 rpm, 10 min, 4°C). The aqueous layer (upper layer) was transferred into a new microcentrifuge tube. 400 µL of chloroform was added and the tube was vortexed for 10 sec. The solution was centrifuged again (13,000 rpm, 10 min, 4°C), and the chloroform extraction was repeated. The aqueous layer was transferred into a clean microcentrifuge tube, then 1/10 volume of 3M sodium acetate (pH 5.5) and 2.5 volumes of cold 100% EtOH were added. The tubes were mixed by inversion and placed at -80°C for ≥ 1 hr. The tubes were centrifuged (13,000 rpm, 10 min, 4°C) and the supernatant was removed. 500 µL of cold 70% EtOH was added, and the tubes were once again centrifuged (13,000 rpm, 10 min, 4°C). The supernatant was removed, and the tubes were left open for 5 min to evaporate remaining EtOH. The pellet was resuspended in 20 µL of water and stored at -80°C.

Using the SequaGel 19:1 Denaturing Gel System (National Diagnostics), an 8% TBE-Urea gel was cast. The gel was pre-run at 45 mA for 30 min. Between 21 and 100 µg of the mitochondrially-enriched RNA was combined with an equal volume of 2X RNA Loading Dye (NEB) and incubated at 70°C for 8 min to denature RNA secondary structure. The samples were loaded onto the gel, which ran at 60 mA for 1 hr in 1X TBE (pH 8.3). The gel was removed from the apparatus, stained with SYBR Gold (Invitrogen) for 10 min, and imaged with an Amersham Typhoon (Cytiva). The tRNA was detected by UV-shadowing and gel segments containing RNA ~70–100 nt in length were excised. The gel slices were placed into microcentrifuge tubes containing 450 µL of 0.3 M NaCl and incubated overnight at 4°C on a tube inverter. The next day, the liquid was transferred to a new microcentrifuge tube and 1.05 mL of 100% EtOH was added. The samples were incubated at -80°C for ≥ 1 h and centrifuged (13,000 rpm, 30 min, 4°C). The supernatant was removed, and the pellet was air dried for 5 min to evaporate remaining EtOH. The pellet was resuspended in 10 µL of water, the RNA concentration was measured using the Qubit RNA BR assay kit (Thermo Fisher Scientific), and the tRNA was stored at -80°C.

tRNA used in APM-PAGE experiments was isolated using Nucleobond AX-100 columns (MachereyNagel) as previously described (Alings et al. 2015).

Nanopore mt-tRNA sequencing

The RNA and DNA oligonucleotides for the splint adapters were ordered from IDT. Separate 10µM (7.5µM for ACCA) stock solutions of the four double-stranded splint adapters were assembled in 1X TNE (10 mM Tris, 50 mM NaCl, 1 mM EDTA) by combining equimolar concentrations of the common adapter that ligates to the 3´ end of the tRNA, and one of four adapter strands complementary to the 3´ tRNA overhang of ACCA, GCCA, UCCA, or CCA (see Supplemental Table S2 for sequences). The splints were annealed by heating at 75°C for 1 min and then cooling to room temperature by leaving the tubes on the bench for 10 min before placing them on ice.

The library preparation was performed as previously described (Shaw et al. 2024), with a few modifications. Briefly, 250 ng of mitochondrial-enriched tRNA was ligated to four different double-stranded splint adapters specific to ACCA (12 pmol), GCCA (8pmol), UCCA (8 pmol), and CCA (4 pmol) tRNA 3´ overhangs (see Supplemental Table S2 for oligonucleotide sequences). The splint adapter cognate for the CCCA 3´ overhang was excluded as no mitochondrial tRNAs in our reference contain this overhang (Supplemental Table S1). In the first ligation, the splint adapters were ligated to tRNA by T4 RNA Ligase 2 (NEB, stock concentration 10,000 U/ml, a total of 10 units per reaction). The second ligation of the ONT RMX motor adapter to the first ligation product was performed with T4 DNA ligase (NEB, 2,000,000 units/ml). The first and second ligation reaction were each purified with magnetic beads (RNA Clean XP, Beckman Coulter), using 1.8X and 1.5X volume of beads added to the reactions, respectively. The elution of the library, flow cell priming and loading followed the SQK-RNA002 protocol. All sequencing was done on the MinION platform with live basecalling turned off to circumvent MinKnow from discarding reads approximating the length of tRNA reads.

IVT mt-tRNA construction and sequencing

The DNA oligonucleotides for the IVT constructs were purchased from IDT. Their sequences are shown in Supplemental Table S2. Yeast IVT mt-tRNAs were generated using the HiScribe T7 Quick High Yield RNA Synthesis Kit (NEB, E2050), as previously done for yeast cytosolic tRNAs (Shaw et al. 2024).

Bioinformatic methods

Analysis of Nanopore DRS data was done essentially as described (Shaw et al. 2024). Basecalling of ionic current files was performed with Guppy v3.0.3, and the resulting FASTQ files were aligned to a reference—containing all 24 mitochondrial and 42 cytosolic tRNA isoacceptors—using BWA-MEM (parameters '-W 13 -k 6 -x ont2d') (Li 2013). Alignments were filtered using SAMtools (Li et al. 2009) to retain those with a mapping quality score greater than one (Q1). marginAlign and the subprogram marginCaller (Jain et al. 2015) were used to generate alignment and error models, and calculate posterior probabilities, respectively. The IVT alignment model, which was derived from a pooled dataset containing mitochondrial IVT tRNA reads (this study) and cytosolic IVT tRNA reads (Shaw et al. 2024), was used as the 'error model' in marginCaller in all experiments. Heatmaps containing the posterior probabilities were generated using matplotlib (Hunter 2007).

Mismatch probability (P(A')), or the probability of any alternative nucleotide call, is complementary to the reference match probability (P(A)).

$$P(A') = 1 - P(A)$$

Random subsets of 105 Q1 aligned reads per mt-tRNA isoacceptor were ran through marginCaller and used to calculate mismatch probabilities for all experiments. Miscalls were assigned to positions with a mismatch probability of $\geq$ 0.3 for biologically derived mt-tRNA samples. To determine novel Pus2-dependent Ψ sites, positions U_{27}/U_{28} with a mismatch probability $\geq$ 0.3 in wild-type and < 0.3 in *pus2*Δ were considered. Changes in mismatch probability ($P(A')_{\Delta}$) were considered significant if the difference was larger than an empirically determined minimum difference threshold ($P(A')_{\Delta, min}$).

$$P(A')_{\Delta} = |P(A')_{mutant} - P(A')_{wild\text{-}type}|$$

The minimum difference threshold was calculated by taking the mean $P(A')_{\Delta}$ value from the 7 known Ψ_{27}/Ψ_{28} sites (Cappannini et al. 2024) and subtracting 1 standard deviation. The value of this threshold for Pus2 sites was 0.140.

$$P(A')_{\Delta, min} = \mu_{P(A')\Delta} - SD$$

For Dus2 sites, a three-position window centered on U_{20} was examined, but only the position with the largest $P(A')_{\Delta}$ for a given isoacceptor was used in proceeding steps. The minimum difference threshold was calculated as described above from the 16 annotated D_{20} sites, and was determined to be 0.223.

APM-PAGE and Northern Blotting

A denaturing gel containing 8% polyacrylamide, 7.5 M urea, and 0.05% ([*N*-acryloylamino]phenyl)mercuric chloride (APM) was cast and pre-ran at 200V for 15 min in 0.5X TBE. Column-isolated, mitochondria-enriched tRNA samples (50 ng) were mixed with an equal volume of 2X RNA Loading Dye (NEB) and heated at 80˚C for 5 min. Samples were loaded onto the gel, which ran at 200V until the lower dye front ran off. The RNA was transferred onto a neutral nylon membrane (GVS) in a Trans-Blot Turbo Transfer System (Bio-Rad) for 35 min at 400 mA with 0.5X TBE. RNA was crosslinked to the membrane at 0.12 J/cm^2 in a UV Stratalinker 1800 (Stratagene). Blots were pre-hybridized in 12.5 mL hybridization buffer (5X SSC, 0.02 M Na_2HPO_4 (pH7.2), 7% SDS, 2X Denhardt) for 4 hr at 50˚C with 500 μg sheared salmon sperm DNA. The hybridization buffer and sheared salmon sperm DNA was replaced, and 50 pmol of IR-800 labeled DNA probe (IDT) specific to mt-tRNA$^{Lys(UUU)}$ (sequence from (Umeda et al. 2005)) was added. Blots were hybridized in the dark overnight at 50˚C, then washed twice (for 10 min and 30 min) in wash buffer (3X SSC, 0.02 M NaH_2PO_4 (pH7.5), 5% SDS, 10X Denhardt), and once in stringent wash buffer (1X SSC, 10% SDS) for 8 min. IR-800 signals were collected using an Amersham Typhoon (Cytiva) and densitometry was performed in Fiji-ImageJ2 (The Fiji Project).

ACKNOWLEDGEMENTS

We thank Eric Westhof (Université de Strasbourg) for his generous input on optimizing the mt-tRNA structural alignment. We thank Sebastian Leidel (University of Bern) for his sharing and guidance on the tRNA Northern Blot protocol. We thank Ethan Shaw and Hannah Wilson (University of Oregon) for their initial pilot experiment to test enrichment of mt-tRNAs. We thank

Rosalind Carrier and Margarita Rojas (University of Oregon) for their assistance with Northern Blots. We thank Alice Barkan (University of Oregon) for comments on the manuscript.

FUNDING

This work was supported by National Institutes of Health grants [R35 GM143125] and [R01 HG013876] to [D.M.G.], and [T32GM149387] to [J.L.R.].

CONFLICTS OF INTEREST

There are no conflicts of interest to report.

REFERENCES

Alfonzo JD, Söll D. 2009. Mitochondrial tRNA import – the challenge to understand has just begun. Biol Chem. 390(8):717–722. doi:10.1515/BC.2009.101.

Alings F, Sarin LP, Fufezan C, Drexler HCA, Leidel SA. 2015. An evolutionary approach uncovers a diverse response of tRNA 2-thiolation to elevated temperatures in yeast. RNA. 21(2):202–212. doi:10.1261/rna.048199.114.

Barraud P, Gato A, Heiss M, Catala M, Kellner S, Tisné C. 2019. Time-resolved NMR monitoring of tRNA maturation. Nat Commun. 10(1):3373. doi:10.1038/s41467-019-11356-w.

Baruffini E, Dallabona C, Invernizzi F, Yarham JW, Melchionda L, Blakely EL, Lamantea E, Donnini C, Santra S, Vijayaraghavan S, et al. 2013. MTO1 Mutations are Associated with Hypertrophic Cardiomyopathy and Lactic Acidosis and Cause Respiratory Chain Deficiency in Humans and Yeast. Hum Mutat. 34(11):1501–1509. doi:10.1002/humu.22393.

Becker HF, Motorin Y, Planta RJ, Grosjean H. 1997. The yeast gene YNL292w encodes a pseudouridine synthase (Pus4) catalyzing the formation of psi55 in both mitochondrial and cytoplasmic tRNAs. Nucleic Acids Res. 25(22):4493–4499. doi:10.1093/nar/25.22.4493.

Begik O, Lucas MC, Pryszcz LP, Ramirez JM, Medina R, Milenkovic I, Cruciani S, Liu H, Vieira HGS, Sas-Chen A, et al. 2021. Quantitative profiling of pseudouridylation dynamics in native RNAs with nanopore sequencing. Nat Biotechnol. 39(10):1278–1291. doi:10.1038/s41587-021-00915-6.

Behm-Ansmant I, Branlant C, Motorin Y. 2007. The Saccharomyces cerevisiae Pus2 protein encoded by YGL063w ORF is a mitochondrial tRNA:Ψ27/28-synthase. RNA. 13(10):1641–1647. doi:10.1261/rna.605607.

Brennan T, Sundaralingam M. 1976. Structure of transfer RNA molecules containing the long variable loop. Nucleic Acids Res. 3(11):3235–3250. doi:10.1093/nar/3.11.3235.

Bullerwell CE, Gray MW. 2004. Evolution of the mitochondrial genome: protist connections to animals, fungi and plants. Curr Opin Microbiol. 7(5):528–534. doi:10.1016/j.mib.2004.08.008.

Canaday J, Dirheimer G, Martin RP. 1980. Yeast mitochondrial methionine initiator tRNA: characterization and nucleotide sequence. Nucleic Acids Res. 8(7):1445–1457. doi:10.1093/nar/8.7.1445.

Cappannini A, Ray A, Purta E, Mukherjee S, Boccaletto P, Moafinejad SN, Lechner A, Barchet C, Klaholz BP, Stefaniak F, et al. 2024. MODOMICS: a database of RNA

modifications and related information. 2023 update. Nucleic Acids Res. 52(D1):D239–D244. doi:10.1093/nar/gkad1083.

Dalluge JJ, Hashizume T, Sopchik AE, McCloskey JA, Davis DR. 1996. Conformational flexibility in RNA: the role of dihydrouridine. Nucleic Acids Res. 24(6):1073–1079.

Di Bartolomeo F, Malina C, Campbell K, Mormino M, Fuchs J, Vorontsov E, Gustafsson CM, Nielsen J. 2020. Absolute yeast mitochondrial proteome quantification reveals trade-off between biosynthesis and energy generation during diauxic shift. Proc Natl Acad Sci. 117(13):7524–7535. doi:10.1073/pnas.1918216117.

Draycott AS, Schaening-Burgos C, Rojas-Duran MF, Wilson L, Schärfen L, Neugebauer KM, Nachtergaele S, Gilbert WV. 2022. Transcriptome-wide mapping reveals a diverse dihydrouridine landscape including mRNA. PLOS Biol. 20(5):e3001622. doi:10.1371/journal.pbio.3001622.

Dyubankova N, Sochacka E, Kraszewska K, Nawrot B, Herdewijn P, Lescrinier E. 2015. Contribution of dihydrouridine in folding of the D-arm in tRNA. Org Biomol Chem. 13(17):4960–4966. doi:10.1039/C5OB00164A.

Ellis SR, Morales MJ, Li JM, Hopper AK, Martin NC. 1986. Isolation and characterization of the TRM1 locus, a gene essential for the N2,N2-dimethylguanosine modification of both mitochondrial and cytoplasmic tRNA in Saccharomyces cerevisiae. J Biol Chem. 261(21):9703–9709.

Fernandez-Vizarra E, Berardinelli A, Valente L, Tiranti V, Zeviani M. 2007. Nonsense mutation in pseudouridylate synthase 1 (PUS1) in two brothers affected by myopathy, lactic acidosis and sideroblastic anaemia (MLASA). J Med Genet. 44(3):173–180. doi:10.1136/jmg.2006.045252.

Gregg C, Kyryakov P, Titorenko VI. 2009. Purification of Mitochondria from Yeast Cells. J Vis Exp JoVE.(30):1417. doi:10.3791/1417.

Han L, Phizicky EM. 2018. A rationale for tRNA modification circuits in the anticodon loop. RNA. 24(10):1277–1284. doi:10.1261/rna.067736.118.

Hunter JD. 2007. Matplotlib: A 2D Graphics Environment. Comput Sci Eng. 9:90–95. doi:10.1109/MCSE.2007.55.

Huot JL, Enkler L, Megel C, Karim L, Laporte D, Becker HD, Duchêne A-M, Sissler M, Maréchal-Drouard L. 2014. Idiosyncrasies in decoding mitochondrial genomes. Biochimie. 100:95–106. doi:10.1016/j.biochi.2014.01.004.

Jain M, Fiddes IT, Miga KH, Olsen HE, Paten B, Akeson M. 2015. Improved data analysis for the MinION nanopore sequencer. Nat Methods. 12(4):351–356. doi:10.1038/nmeth.3290.

Kamenski P, Kolesnikova O, Jubenot V, Nina Entelis, Krasheninnikov IA, Martin RP, Tarassov I. 2007. Evidence for an adaptation mechanism of mitochondrial translation via tRNA import from the cytosol. Mol Cell. 26(5):625–637. doi:10.1016/j.molcel.2007.04.019.

Kilz L-M, Zimmermann S, Marchand V, Bourguignon V, Sudol C, Brégeon D, Hamdane D, Motorin Y, Helm M. 2024 Oct 26. Differential redox sensitivity of tRNA dihydrouridylation. Nucleic Acids Res.:gkae964. doi:10.1093/nar/gkae964.

Koster CC, Kleefeldt AA, van den Broek M, Luttik M, Daran J-M, Daran-Lapujade P. 2024. Long-read direct RNA sequencing of the mitochondrial transcriptome of Saccharomyces cerevisiae reveals condition-dependent intron abundance. Yeast. 41(4):256–278. doi:10.1002/yea.3893.

Krahn N, Fischer JT, Söll D. 2020. Naturally Occurring tRNAs With Non-canonical Structures. Front Microbiol. 11. [accessed 2024 Feb 6]. https://www.frontiersin.org/journals/microbiology/articles/10.3389/fmicb.2020.596914.

Li H. 2013. Aligning sequence reads, clone sequences and assembly contigs with BWA-MEM. doi:10.48550/arXiv.1303.3997. [accessed 2024 Oct 14]. http://arxiv.org/abs/1303.3997.

Li H, Handsaker B, Wysoker A, Fennell T, Ruan J, Homer N, Marth G, Abecasis G, Durbin R. 2009. The Sequence Alignment/Map format and SAMtools. Bioinformatics. 25(16):2078–2079. doi:10.1093/bioinformatics/btp352.

Lucas MC, Pryszcz LP, Medina R, Milenkovic I, Camacho N, Marchand V, Motorin Y, Ribas De Pouplana L, Novoa EM. 2023 Apr 6. Quantitative analysis of tRNA abundance and modifications by nanopore RNA sequencing. Nat Biotechnol. doi:10.1038/s41587-023-01743-6. [accessed 2023 Jun 21]. https://www.nature.com/articles/s41587-023-01743-6.

Machnicka MA, Olchowik A, Grosjean H, Bujnicki JM. 2015. Distribution and frequencies of post-transcriptional modifications in tRNAs. RNA Biol. 11(12):1619–1629. doi:10.4161/15476286.2014.992273.

Magistrati M, Gilea AI, Ceccatelli Berti C, Baruffini E, Dallabona C. 2023. Modopathies Caused by Mutations in Genes Encoding for Mitochondrial RNA Modifying Enzymes: Molecular Mechanisms and Yeast Disease Models. Int J Mol Sci. 24(3):2178. doi:10.3390/ijms24032178.

Mangum JE, Hardee JP, Fix DK, Puppa MJ, Elkes J, Altomare D, Bykhovskaya Y, Campagna DR, Schmidt PJ, Sendamarai AK, et al. 2016. Pseudouridine synthase 1 deficient mice, a model for Mitochondrial Myopathy with Sideroblastic Anemia, exhibit muscle morphology and physiology alterations. Sci Rep. 6(1):26202. doi:10.1038/srep26202.

Meisinger C, Pfanner N, Truscott KN. 2005. Isolation of Yeast Mitochondria. Methods Mol Biol. 313:033–040. doi:10.1385/1-59259-958-3:033.

Metodiev MD, Assouline Z, Landrieu P, Chretien D, Bader-Meunier B, Guitton C, Munnich A, Rötig A. 2015. Unusual clinical expression and long survival of a pseudouridylate synthase (PUS1) mutation into adulthood. Eur J Hum Genet. 23(6):880–882. doi:10.1038/ejhg.2014.192.

Miyakawa I, Miyamoto M, Kuroiwa T, Sando N. 2004. DNA Content of Individual Mitochondrial Nucleoids Varies Depending on the Culture Conditions of the Yeast Saccharomyces cerevisiae. Cytologia (Tokyo). 69(1):101–107. doi:10.1508/cytologia.69.101.

Morgenstern M, Stiller SB, Lübbert P, Peikert CD, Dannenmaier S, Drepper F, Weill U, Höß P, Feuerstein R, Gebert M, et al. 2017. Definition of a High-Confidence Mitochondrial Proteome at Quantitative Scale. Cell Rep. 19(13):2836. doi:10.1016/j.celrep.2017.06.014.

Motorin Y, Keith G, Simon C, Foiret D, Simos G, Hurt E, Grosjean H. 1998. The yeast tRNA:pseudouridine synthase Pus1p displays a multisite substrate specificity. RNA N Y N. 4(7):856–869. doi:10.1017/s1355838298980396.

Nomura Y, Ohno S, Nishikawa K, Yokogawa T. 2016. Correlation between the stability of tRNA tertiary structure and the catalytic efficiency of a tRNA-modifying enzyme, archaeal tRNA-guanine transglycosylase. Genes Cells Devoted Mol Cell Mech. 21(1):41–52. doi:10.1111/gtc.12317.

Patton JR, Bykhovskaya Y, Mengesha E, Bertolotto C, Fischel-Ghodsian N. 2005. Mitochondrial Myopathy and Sideroblastic Anemia (MLASA): MISSENSE MUTATION IN THE PSEUDOURIDINE SYNTHASE 1 (PUS1) GENE IS ASSOCIATED WITH THE LOSS OF tRNA PSEUDOURIDYLATION *. J Biol Chem. 280(20):19823–19828. doi:10.1074/jbc.M500216200.

Percudani R, Pavesi A, Ottonello S. 1997. Transfer RNA gene redundancy and translational selection in Saccharomyces cerevisiae. J Mol Biol. 268(2):322–330. doi:10.1006/jmbi.1997.0942.

Phizicky EM, Hopper AK. 2023. The life and times of a tRNA. RNA. 29(7):898–957. doi:10.1261/rna.079620.123.

Porat J. 2025. Circuit logic: interdependent RNA modifications shape mRNA and noncoding RNA structure and function. RNA. 31(5):613–622. doi:10.1261/rna.080421.125.

Powell CA, Kopajtich R, D'Souza AR, Rorbach J, Kremer LS, Husain RA, Dallabona C, Donnini C, Alston CL, Griffin H, et al. 2015. TRMT5 Mutations Cause a Defect in Post-transcriptional Modification of Mitochondrial tRNA Associated with Multiple Respiratory-Chain Deficiencies. Am J Hum Genet. 97(2):319–328. doi:10.1016/j.ajhg.2015.06.011.

Rinehart J, Krett B, Rubio MAT, Alfonzo JD, Söll D. 2005. Saccharomyces cerevisiae imports the cytosolic pathway for Gln-tRNA synthesis into the mitochondrion. Genes Dev. 19(5):583–592. doi:10.1101/gad.1269305.

Riquelme-Barrios S, Vásquez-Camus L, Cusack SA, Burdack K, Petrov DP, Yeşiltaç-Tosun GN, Kaiser S, Giehr P, Jung K. 2025. Direct RNA sequencing of the Escherichia coli epitranscriptome uncovers alterations under heat stress. Nucleic Acids Res. 53(6):gkaf175. doi:10.1093/nar/gkaf175.

Rubio MAT, Hopper AK. 2011. tRNA travels from the cytoplasm to organelles. Wiley Interdiscip Rev RNA. 2(6):802–817. doi:10.1002/wrna.93.

Salinas-Giegé T, Giegé R, Giegé P. 2015. tRNA Biology in Mitochondria. Int J Mol Sci. 16(3):4518. doi:10.3390/ijms16034518.

Sayers EW, Beck J, Bolton EE, Brister JR, Chan J, Comeau DC, Connor R, DiCuccio M, Farrell CM, Feldgarden M, et al. 2024. Database resources of the National Center for Biotechnology Information. Nucleic Acids Res. 52(D1):D33–D43. doi:10.1093/nar/gkad1044.

Schneller JM, Schneller C, Martin R, Stahl AJ. 1976. Nuclear origin of specific yeast mitochondrial aminoacyl-tRNA synthetases. Nucleic Acids Res. 3(5):1151–1165. doi:10.1093/nar/3.5.1151.

Shaw EA, Thomas NK, Jones JD, Abu-Shumays RL, Vaaler AL, Akeson M, Koutmou KS, Jain M, Garcia DM. 2024. Combining Nanopore direct RNA sequencing with genetics and mass spectrometry for analysis of T-loop base modifications across 42 yeast tRNA isoacceptors. Nucleic Acids Res.:gkae796. doi:10.1093/nar/gkae796.

Sibler A-P, Dirheimer G, Martin RP. 1981. Nucleotide sequence of a yeast mitochondrial threonine-tRNA able to decode the C—U—N leucine codons. FEBS Lett. 132(2):344–348. doi:10.1016/0014-5793(81)81194-5.

Steinberg S, Misch A, Sprinzl M. 1993. Compilation of tRNA sequences and sequences of tRNA genes. Nucleic Acids Res. 21(13):3011–3015.

Su D, Lieberman A, Lang BF, Simonović M, Söll D, Ling J. 2011. An unusual tRNAThr derived from tRNAHis reassigns in yeast mitochondria the CUN codons to threonine. Nucleic Acids Res. 39(11):4866–4874. doi:10.1093/nar/gkr073.

Sun Y, Piechotta M, Naarmann-de Vries I, Dieterich C, Ehrenhofer-Murray AE. 2023. Detection of queuosine and queuosine precursors in tRNAs by direct RNA sequencing. Nucleic Acids Res. 51(20):11197–11212. doi:10.1093/nar/gkad826.

Suzuki T. 2021. The expanding world of tRNA modifications and their disease relevance. Nat Rev Mol Cell Biol. 22(6):375–392. doi:10.1038/s41580-021-00342-0.

Suzuki Takeo, Yashiro Y, Kikuchi I, Ishigami Y, Saito H, Matsuzawa I, Okada S, Mito M, Iwasaki S, Ma D, et al. 2020. Complete chemical structures of human mitochondrial tRNAs. Nat Commun. 11(1):4269. doi:10.1038/s41467-020-18068-6.

Tarassov I, Entelis N, Martin RP. 1995. Mitochondrial import of a cytoplasmic lysine-tRNA in yeast is mediated by cooperation of cytoplasmic and mitochondrial lysyl-tRNA synthetases. EMBO J. 14(14):3461–3471.

Thomas NK, Poodari VC, Jain M, Olsen HE, Akeson M, Abu-Shumays RL. 2021. Direct Nanopore Sequencing of Individual Full Length tRNA Strands. ACS Nano. 15(10):16642–16653. doi:10.1021/acsnano.1c06488.

Turk EM, Das V, Seibert RD, Andrulis ED. 2013. The Mitochondrial RNA Landscape of Saccharomyces cerevisiae. PLOS ONE. 8(10):e78105. doi:10.1371/journal.pone.0078105.

Umeda N, Suzuki Takeo, Yukawa M, Ohya Y, Shindo H, Watanabe K, Suzuki Tsutomu. 2005. Mitochondria-specific RNA-modifying Enzymes Responsible for the Biosynthesis of the Wobble Base in Mitochondrial tRNAs: IMPLICATIONS FOR THE MOLECULAR PATHOGENESIS OF HUMAN MITOCHONDRIAL DISEASES *. J Biol Chem. 280(2):1613–1624. doi:10.1074/jbc.M409306200.

Wang X, Yan Q, Guan M-X. 2009. Mutation in MTO1 involved in tRNA modification impairs mitochondrial RNA metabolism in the yeast Saccharomyces cerevisiae. Mitochondrion. 9(3):180–185. doi:10.1016/j.mito.2009.01.010.

Wang X, Yan Q, Guan M-X. 2010. Combination of the loss of cmnm5U34 with the lack of s2U34 modifications of tRNALys, tRNAGlu and tRNAGln altered mitochondrial biogenesis and respiration. J Mol Biol. 395(5):1038. doi:10.1016/j.jmb.2009.12.002.

White LK, Dobson K, Pozo S del, Bilodeaux JM, Andersen SE, Baldwin A, Barrington C, Körtel N, Martinez-Seidel F, Strugar SM, et al. 2024. Comparative analysis of 43 distinct RNA modifications by nanopore tRNA sequencing. :2024.07.23.604651. doi:10.1101/2024.07.23.604651. [accessed 2024 Oct 14]. https://www.biorxiv.org/content/10.1101/2024.07.23.604651v1.

White LK, Strugar SM, MacFadden A, Hesselberth JR. 2023. Nanopore sequencing of internal 2'-PO4 modifications installed by RNA repair. RNA N Y N. 29(6):847–861. doi:10.1261/rna.079290.122.

Wolters JF, Chiu K, Fiumera HL. 2015. Population structure of mitochondrial genomes in Saccharomyces cerevisiae. BMC Genomics. 16(1):451. doi:10.1186/s12864-015-1664-4.

Xing F, Hiley SL, Hughes TR, Phizicky EM. 2004. The Specificities of Four Yeast Dihydrouridine Synthases for Cytoplasmic tRNAs * [boxs]. J Biol Chem. 279(17):17850–17860. doi:10.1074/jbc.M401221200.

Yared M-J, Yoluç Y, Catala M, Tisné C, Kaiser S, Barraud P. 2023. Different modification pathways for m1A58 incorporation in yeast elongator and initiator tRNAs. Nucleic Acids Res. 51(19):10653–10667. doi:10.1093/nar/gkad722.